

Model simulations of dust sources and transport in the global atmosphere: Effects of soil erodibility and wind speed variability

Alf Grini,^{1,2} Gunnar Myhre,¹ Charles S. Zender,³ and Ivar S. A. Isaksen¹

Received 19 May 2004; revised 21 October 2004; accepted 18 November 2004; published 25 January 2005.

[1] Global atmospheric dust is simulated using the Dust Entrainment and Deposition (DEAD) model in combination with the global-scale Oslo chemical transport model CTM2 using meteorological data for 1996. Dust sources are calculated using both mean wind speeds with model resolution T63 and subgrid wind speeds. Different data sets are used to describe soil erodibility. We explain how the different assumptions about dust production affect atmospheric dust burden and deposition. Some aspects of the annual dust cycle, such as the east Asian dust emissions, are largely dependent on the data used to determine soil erodibility. Other aspects, such as the timing of the maximum in the African plume at Northern Hemisphere summer, are well modeled with all data sets applied here. We show that the daily variation in optical depth at Cape Verde on the west coast of Africa is well simulated when we assume that erodibility is correlated with surface reflectivity from Moderate-Resolution Imaging Spectroradiometer (MODIS) satellite data. Using a subgrid probability density function of wind speed to drive the dust sources facilitates dust emissions in areas with low wind speeds. Dust concentrations in remote areas are sensitive to the parameterization of wet deposition. Our results point out the need for a detailed soil erodibility data set for global dust modeling, and they suggest that surface reflectivity is potentially valuable for producing or evaluating such data sets.

Citation: Grini, A., G. Myhre, C. S. Zender, and I. S. A. Isaksen (2005), Model simulations of dust sources and transport in the global atmosphere: Effects of soil erodibility and wind speed variability, *J. Geophys. Res.*, *110*, D02205, doi:10.1029/2004JD005037.

1. Introduction

[2] Atmospheric mineral dust plays many roles in Earth's climate system, including the radiation budget [Myhre and Stordal, 2001], atmospheric photochemistry [Bian and Zender, 2003], cloud condensation nuclei and ice nuclei [Lohmann, 2002], stratospheric water vapor [Sherwood, 2002] and nutrient transport to oceans and forests [Prospero, 1996].

[3] Before analyzing in detail the effects of these processes on climate, it is important to understand the production, transport, and loss of mineral dust in the global atmosphere. In this study, we focus on how different assumptions about dust production affect the atmospheric dust loading and deposition fluxes.

[4] Several modeling studies have tried to quantify the global production and transport of atmospheric mineral dust [Tegen and Fung, 1994; Claquin, 1999; Ginoux *et al.*, 2001; Woodward, 2001; Zender *et al.*, 2003a]. Early estimates for global production lie in the range 500–5000 Tg yr⁻¹.

[5] It has become clear that deserts are not homogeneous dust sources. Dust is emitted from hot spots or preferential source regions. Gillette [1999] considered in detail all the factors that could possibly cause a desert region to be a preferential dust source. Some of the most important factors were (1) high wind speeds, (2) lack of nonerodible roughness elements, (3) low threshold wind velocity, (4) lack of aggregation or crusting, (5) high particle availability, and (6) low binding energies of the suspended particles in the soil matrix.

[6] The review article by Prospero *et al.* [2002] described in detail preferential source regions around the world. They found that dust hot spots are usually associated with topographical lows and that most major sources had been flooded some time during the last 2 million years. They proposed that hot spots are areas where alluvial dust particles are available for erosion. For example, the Takla Makan Desert in the Chinese Tarim basin would have

¹Department of Geosciences, University of Oslo, Oslo, Norway.

²Department of Physical Sciences, University of Helsinki, Helsinki, Finland.

³Department of Earth System Science, University of California, Irvine, California, USA.

several hundred meters of deposits available for erosion. A natural conclusion to draw from *Prospero et al.* [2002] is that high particle availability is the most important reason for dust hot spots. An observational study by *Mahowald et al.* [2003] confirmed that ephemeral lakes emitted more dust than neighboring areas.

[7] Several modeling studies have tried to incorporate these findings into their dust production models. *Ginoux et al.* [2001] made a simple erodibility factor based on a topographical map to make topographical lows emit more dust than other areas for the same wind friction speeds. This assumption improved their predictions compared to not taking into account differences in soil erodibility. *Tegen et al.* [2002] simulated soil erodibility using a water routing and storage model to obtain soil erodibility. *Zender et al.* [2003b] calculated soil erodibility by assuming it was proportional to the upstream area from which sediments may have accumulated locally through all climate regimes. A soil erodibility parameter in global dust production models complicates the question of anthropogenic dust emissions since humans influence not only vegetation and surface conditions but also surface hydrology and the hydrological cycle.

[8] This study applies a three-dimensional transport model to describe the annual dust cycle. We focus on two aspects of dust production modeling: soil erodibility and wind speed variability.

[9] *Schaaf et al.* [2002] showed how the Moderate-Resolution Imaging Spectroradiometer (MODIS) satellite can retrieve specific land types on the basis of surface reflection. Surface reflection is largely dependent on soil types, and *Tsvetsinskaya et al.* [2002] point out that sand dunes have the highest surface reflectivity of all surface types. Sand dunes will be efficient dust producers if a sufficient fraction of their saltation-sized particles are aggregates or if a sufficient amount of interstitial clay-size particles are present. Therefore we would like to find out whether areas with high reflectivity also are areas with high erodibility. We introduce two new erodibility factors based on MODIS surface reflection and compare them to model results using the earlier published erodibility factors.

[10] We explore the importance of using a probability density function of wind speeds. We model dust production both with a parameterization taking wind speed variability into account [*Justus et al.*, 1978] and with a parameterization using winds at model resolution. The difference between these simulations shows the sensitivity to neglecting subgrid-scale wind speed variability in dust production models.

2. Modeling

2.1. Dust Production

[11] Dust emissions are modeled using the Dust Entrainment and Deposition (DEAD) model [*Zender et al.*, 2003a]. This model is based on the work of *Martcorena and Bergametti* [1995]. Emissions start when wind friction speeds reach a threshold of approximately 0.2 m s^{-1} [*Iversen and White*, 1982]. A horizontal saltation (soil) flux and a vertical (dust) flux are calculated. The size distribution of the vertical dust flux is distributed to three modes according to *D'Almeida* [1987]. The most important mode

(96% of the mass) has a mass median diameter (MMD) of $4.82 \mu\text{m}$.

[12] Two factors modify the dust production: (1) a global tuning factor, T (this factor is determined “a posteriori” and ensures that global emissions in all simulations are the same; T is a global constant), and (2) an erodibility factor, RDBFCT (this factor is described in detail below; the factor is meant to take into account the fact that some desert surfaces are easier to erode than others [*Prospero et al.*, 2002]).

[13] The total emissions in a given grid are thus

$$\text{EM} = \text{EM}_{\text{phys}} \times \text{RDBFCT} \times T, \quad (1)$$

where EM_{phys} corresponds to the emissions modeled by the equations of the production module and EM is total emissions.

2.2. Soil Erodibility

[14] In this study, we use four different erodibility factors to simulate dust production. Two of them are already published [*Ginoux et al.*, 2001; *Zender et al.*, 2003b]. *Ginoux et al.* [2001] applied the idea that wherever there are large basins in the world, rivers and lakes would have accumulated loess and sand to give large erodibility. This reasoning led to the following formulation for erodibility factor:

$$\text{TOPO} = \left(\frac{z_{\text{max}} - z}{z_{\text{max}} - z_{\text{min}}} \right)^5, \quad (2)$$

where TOPO is the erodibility factor, z is the elevation of the grid point, and z_{min} and z_{max} are the lowest and highest points in the surrounding $10^\circ \times 10^\circ$ area.

[15] *Zender et al.* [2003b] calculated the erodibility assuming it was proportional to the upstream area from which sediments may have accumulated locally during different climate regimes. Using a global transport model, they found that overall correlation with measurements improved with their geomorphological erodibility factor (GEO) relative to TOPO [*Ginoux et al.*, 2001].

[16] We introduce two new erodibility factors, which are based on the assumption that erodibility is correlated with surface reflectance. We used the data set MOD09 [*Schaaf et al.*, 2002] from the MODIS satellite to produce these two new erodibility factors: MDLNR and MDSSQR. The factor MDLNR is calculated according to equation (3), and MDSSQR is calculated according to equation (4). The erodibility described by MDLNR is the base case in this work.

$$\text{MDLNR}(i,j) = \frac{\text{SR}(i,j)}{\text{SR}_{\text{max}}}, \quad (3)$$

$$\text{MDSSQR}(i,j) = \frac{\text{SR}(i,j)^2}{\text{SR}_{\text{max}}^2}, \quad (4)$$

where SR means surface reflectance and SR_{max} is the maximum surface reflectance that is situated in the Sahara. The yearly average surface reflectance was calculated

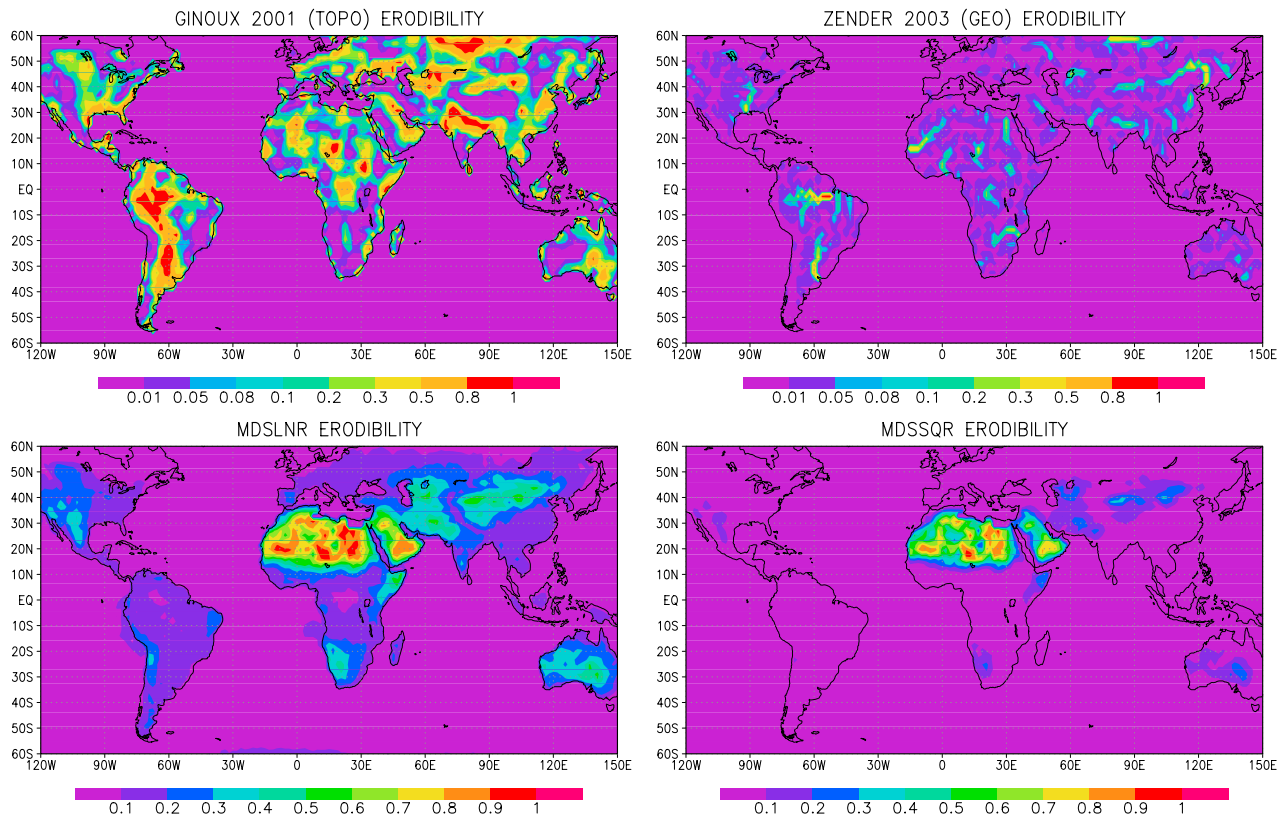


Figure 1. Erodibility factors obtained by four different methods. Upper left is the method of *GINoux et al.* [2001] (TOPO), upper right is the method of *Zender et al.* [2003b] (GEO), lower left is the factor described in equation (3) (MDLNR), and lower right is the factor described in equation (4) (MDSSQR). Note that the images have different color scales because of very different values and gradients in the data.

averaging monthly mean data downloaded from ftp://modis.gsfc.nasa.gov/outgoing/Data_Sets/CD/land/HDF/SURFACE_REFLECTANCE/. We used data from channel 7 since these data use a “fill value” (rather than a high reflectivity) for snow cover [*Schaaf et al.*, 2002]. This keeps snow areas from being considered as dust emitters.

[17] Equations (3) and (4) are very simple concepts for erodibility data sets. They take into account that sand dunes have high reflectivity. At the same time, we assume that sand dunes also have high erodibility. These factors thus indicate where sand dunes are available for erosion. Both MODIS data sets give the same areas as preferential sources, but MDSSQR has larger gradients between preferential source areas and other areas. MDSSQR is thus more spatially heterogeneous than MDLNR. Areas with medium reflectivity get low erodibility when using MDSSQR since the difference from areas with high reflectivity increases. We compare the erodibility factors in Figure 1.

[18] Figure 1 shows that the different erodibility data sets have very different values and gradients (note the different color scales used in the figure). In the Sahara, all four data sets impose high erodibility in the west (Mali/Mauritania/Algeria), southeast (Lake Chad), and east (Egypt/Libya/Sudan/Chad). Even though the placements show similarities, both TOPO and GEO show high erodibility in Mauritania farther west than MODIS, which has highest reflectance in a

square between (12°W, 17°N) and (3°W, 22°N). In the eastern Sahara, TOPO does not predict the same area as MDLNR/MDSSQR and GEO. TOPO predicts high erodibility in a small area in northeastern Libya, and GEO predicts high erodibility along the Nile River.

[19] In east Asia, MDLNR and MDSSQR give low erodibility in both Takla Makan and Gobi Deserts compared to GEO and TOPO. However, the geographical placement of the maximum is approximately equal in all data sets.

[20] In Arabia, all data sets agree on high erodibility in southern Saudi Arabia. MDLNR/MDSSQR give high erodibility in northern Saudi Arabia too, whereas both TOPO and GEO give a maximum in Iraq along the Tigris/Euphrates river basin that is not indicated by MDLNR/MDSSQR.

[21] In Australia, all data sets propose higher erodibility in the Lake Eyre basin (southeast) compared to the Great Sandy Desert (northwest).

2.3. Soil Moisture

[22] Soil moisture inhibits dust production [*Fecan et al.*, 1999]. Soil moisture in desert areas is very low. The parameterization of evaporation used in the ECMWF model [*Viterbo and Beljaars*, 1995] does not capture variations in soil moisture at the scale described by *Fecan et al.* [1999]. Evaporation from soils in the ECMWF model stops at a globally constant permanent wilting point of $0.171 \text{ m}^3 \text{ m}^{-3}$.

This soil moisture is too high to describe soil moisture variations in deserts.

[23] Instead of tuning the *Fecan et al.* [1999] parameterizations to fit the ECMWF soil moisture, we have chosen to use a simplified approach based on rainfall. Our approach takes into account two factors: (1) After a rainfall, the soil has to dry before it can start producing dust. (2) The soil needs more time to dry after a large rainfall than after a small rainfall. The time required by the soil to dry depends on air temperature, humidity, surface winds, and soil texture. To implement these processes, we need to build a whole new soil moisture model, which is beyond the scope of this study. To get around the problem, we made the following simple assumptions: (1) The production of dust is stopped if precipitation during the last 24 hours is larger than 0.50 mm; (2) the length of the period without emissions (in days) is equal to the amount of rain during the last 24 hours (in mm); and (3) if no rain has fallen in the last 5 days, the soil is assumed to be dry no matter the size of the last rainfall. A similar approach has been used by *Claquin* [1999] and *Myhre et al.* [2003].

2.4. Probability Density Function of Wind Speeds

[24] We use a probability density function (PDF) of winds speeds proposed by *Justus et al.* [1978] to drive dust emissions. The Weibull distribution is described by a shape factor (k) and a scale factor (c). The factors are calculated from wind speed at reference height (10 m) from equations (5) and (6).

$$k_{\text{ref}} = 0.94 \sqrt{U_{\text{ref}}}, \quad (5)$$

where k_{ref} is the Weibull distribution shape factor and U_{ref} is the wind speed at reference height

$$c_{\text{ref}} = U_{\text{ref}} / \Gamma \left(1 + \frac{1}{k_{\text{ref}}} \right), \quad (6)$$

where c_{ref} is the Weibull distribution scale factor and Γ is the gamma function.

[25] We use a 95th percentile in the distribution, meaning that the lowest wind speed considered is slower than 95% of the winds and the fastest wind speed considered is faster than 95% of the winds. Our earlier paper [*Grini and Zender*, 2004] used the same formulation to study the effect of using wind speed PDF on the dust size distribution. In the present study, the size distribution of the emitted dust is always the same.

[26] There are two important reasons for introducing a subgrid variability. First, it allows emissions from grid cells where the grid cell mean wind is beneath the mobilization threshold.

[27] Second, we believe subgrid wind variability describes more realistically the mobilization physics. For example, it can change timing of the emission events. In the summer afternoon, the ground is heated by solar radiation, giving high wind speeds and turbulence close to the ground. Our formulation allows us to estimate a realistic wind speed variability even though the formulation is not directly linked to turbulent activity and convective energy as was done by *Cakmur et al.* [2004].

2.5. Atmospheric Transport and Meteorological Data

[28] We use the Oslo chemical transport model CTM2 for atmospheric transport [*Sundet*, 1997]. CTM2 has been used for several chemistry and transport studies [*Grini et al.*, 2002; *Myhre et al.*, 2003; *Berglen et al.*, 2004; *Endresen et al.*, 2003; *Gauss et al.*, 2003]. CTM2 is an off-line model driven by ECMWF forecast data. Advection is done with the second-order moment method [*Prather*, 1986]. Convection in CTM2 is based on the mass flux precalculated by the Tiedtke scheme [*Tiedtke*, 1989]. Vertical transport is based on the surplus/deficit in a column.

[29] This study uses meteorological data from the year 1996, the only year for which high-resolution global data were available. We chose to use a year with higher resolution to better capture the high wind speeds responsible for dust emissions. By running only one year, we are unable to capture interannual changes in dust loading, but we believe that we are still able to illustrate the effects of changing assumptions about dust production. According to *Zender et al.* [2003a], the years 1996–1998 were less dusty than the preceding years, 1990–1995.

2.6. Wet Deposition

[30] Wet deposition is a difficult process to model. The hygroscopic properties of dust are not well known and change during transport. Dust may, for example, get coated with water-soluble organics or sulfate, which will make it easier to activate as cloud droplets [*Fan et al.*, 2004]. To calculate the wet deposition accurately, one would need a detailed description of cloud and aerosol microphysics [e.g., *Ghan et al.*, 1998; *Nenes et al.*, 2001].

[31] Because of the complexity of wet deposition, we chose to include a simple size-independent wet deposition scheme. Our model includes two different types of wet deposition.

2.6.1. Large-Scale Wet Deposition

[32] Wet deposition is done using three-dimensional rainfall data and assuming that dust washout is dependent on rainfall, cloud liquid water, and cloud fraction. Re-evaporation is taken into account only if all the rain evaporates.

$$\text{LOSS} = \epsilon * C_{\text{dust}} * \text{CLDFRC} * \frac{\text{RAIN}}{\text{CLDLWC}}, \quad (7)$$

where LOSS is the loss in kg, ϵ is a factor between 0 and 1 describing how easily dust is taken up by the cloud, C_{dust} is dust concentration in kilograms, CLDFRC is the fraction of the grid cell covered by cloud, RAIN is rainfall in the time step (kilograms), and CLDLWC is the cloud liquid water (kilograms). This study uses $\epsilon = 1$. Sensitivity to this choice is discussed briefly in section 3.1.1.

[33] This formulation is well suited for soluble aerosols such as sulfates. However, its validity is more limited when it is used for dust. Some dust can dissolve in water, especially if the dust is rich in carbonates [*Claquin et al.*, 1999], and dust can get coated with water-soluble material. The validity of our formulation thus depends on the mineral content of the dust and on atmospheric composition. It is possible that our formulation of wet deposition is not valid in areas with highly insoluble dust and

Table 1. Description of Model Experiments^a

Run	Erodibility	Winds	Run Name
1	MDSLNR	PDF	MDSLNRPDF
2	MDSSQR	PDF	MDSSQRPDF
3	GEO	PDF	GEOPDF
4	TOPO	PDF	TOPOPDF
5	MDSLNR	mean	MDSLNRMEAN

^aDust production is changed using different assumptions about soil erodibility and wind variability. Experiments 1–4 use different assumptions about soil erodibility (section 2.2) and use subgrid wind speeds to mobilize dust. Experiment 5 uses mean rather than subgrid wind speeds. Differences between simulations 1 and 5 show sensitivity to neglecting wind speed variability.

no possibilities for coating the dust with water-soluble materials.

2.6.2. Convective Wet Deposition

[34] This process removes dust whenever the air rising in a convective tower becomes supersaturated. It is important to couple removal directly to the convective transport so that dust is not first transported to high altitudes by convection before any removal algorithm is applied. After transport, the dust would no longer be available in the clouds to be removed by rain. Convective rain removes dust with an efficiency $\epsilon = 1$ as described for large-scale wet deposition. Convective removal is described in detail by *Berglen et al.* [2004].

2.7. Dry Deposition

[35] Dry deposition uses a resistance method as described by *Zender et al.* [2003a]. The deposition velocity depends on wind friction speed and surface stability. Dry deposition is largest for the large aerosols and the areas with high wind friction speed [*Seinfeld and Pandis*, 1998].

2.8. Description of Model Experiments

[36] Five model experiments were performed. The experiments were normalized using different tuning factors (T) so that all gave the same annual emissions of 1500 Tg yr^{-1} . The reason why we normalized the emissions rather than the loading, as was done by *Zender et al.* [2003b], was that we want to look at how the same amount of emitted dust gets distributed in the atmosphere under different mobilization assumptions shown in Table 1.

[37] Simulations 1–4 use four different descriptions of soil erodibility (RDBFCT in equation (1), see section 2.2): The different erodibility factors used are labeled MDSLNR (equation (3)), MDSSQR (equation (4)), GEO [*Zender et al.*, 2003a], and TOPO (equation (2)). The differences between simulations 1, 2, 3, and 4 show the effect of assuming different placements of erodible soils.

[38] All simulations except simulation 5 (MDSLNRMEAN) use the Weibull distribution to describe the winds used to drive dust production. MDSLNRMEAN uses mean wind speeds at model resolution. The differences between simulations MDSLNRMEAN and MDSLNR show sensitivity to neglecting wind speed variability in dust production. The simulations using Weibull winds are labeled “PDF” in Table 1, and the simulation using mean wind is labeled “mean” in Table 1. The names of the experiments given in this table are used throughout the manuscript.

3. Results and Sensitivity Tests

3.1. General Evaluation of the Oslo CTM2 Dust Model

[39] Before describing in detail the effect of the different dust production formulations, we discuss below the general behavior of the dust mass budget in the Oslo CTM2 model for the MDSLNRPDF experiment.

3.1.1. Global Budgets and Fluxes

[40] Table 2 shows the global fluxes in the different experiments. All experiments are prescribed a total of 1500 Tg yr^{-1} emissions. The loss terms are dominated by dry deposition ($\sim 50\text{--}60\%$), followed by stratiform scavenging ($\sim 30\text{--}40\%$) and convective scavenging ($\sim 10\%$).

[41] Figure 2 shows where the different loss processes are important. Dust close to the arid source regions is mainly lost by dry deposition since precipitation is rare. Wet deposition is more important in remote ocean regions. The dust size distribution changes during transport, so that the largest particles fall out close to source areas and smaller particles are more susceptible to wet deposition. Convective washout is most efficient close to the equator, in the Intertropical Convergence Zone (ITCZ).

[42] In a sensitivity experiment, we ran MDSLNRPDF with parameter ϵ (see section 2.6.1) set to 0.3 to reduce the washout efficiency. This increases the aerosol loading significantly and gives a total load of 29 Tg , an increase of approximately 50%.

3.1.2. Nutrient Budgets

[43] Table 3 shows the yearly deposition to different ocean and forest regions. An increasing interest in the role of dust in transport of trace metals in the atmosphere has made it interesting for dust modelers to compare their fluxes to estimates given in the literature for model evaluation purposes. All our simulations yield approximately 400 Tg yr^{-1} deposition to the oceans. *Zender et al.* [2003a] calculated a total flux of 315 Tg yr^{-1} , and *Prospero* [1996] gives values between 358 Tg yr^{-1} and 910 Tg yr^{-1} .

Table 2. Global Budget for Deposition Fluxes and Burden^a

Run	DRYDEP, %	LS WETDEP, %	CNV WETDEP, %	Burden, Tg
MDSLNRPDF	52.9	36.3	10.8	18.9
MDSSQRPDF	53.2	36.1	10.7	19.5
GEOPDF	54.1	35.1	10.8	19.2
TOPOPDF	53.3	35.2	11.5	16.3
MDSLNRMEAN	52.0	37.2	10.8	17.4

^aFluxes are expressed as percentage of total mass flux. Annual total production is 1500 Tg . Burden is given in Tg. DRYDEP is dry deposition flux (section 2.7), and LS WETDEP and CNV WETDEP are large-scale (section 2.6.1) and convective (section 2.6.2) wet deposition fluxes, respectively.

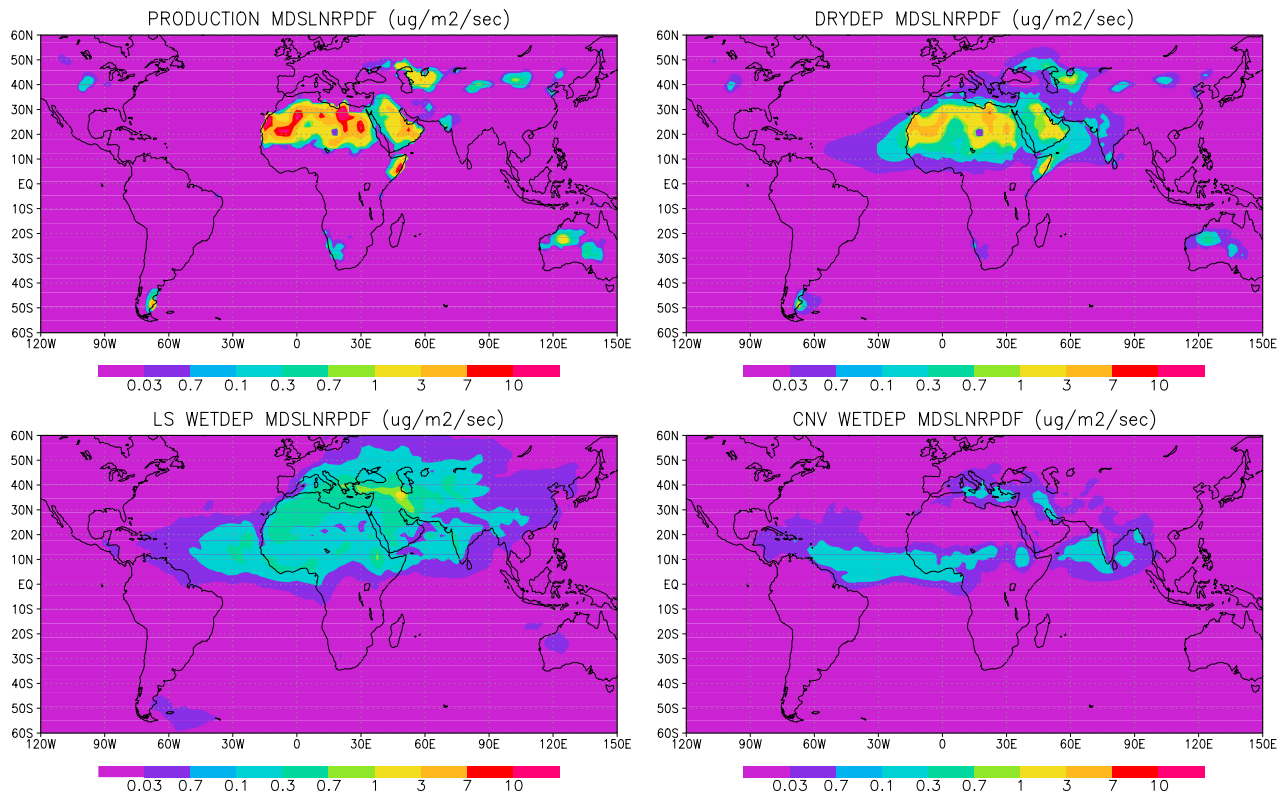


Figure 2. Loss processes for MDSLNRPDF experiment. Shown are annual mean production, dry deposition, large-scale rainout, and convective rainout. All fluxes are in $\mu\text{g m}^{-2} \text{s}^{-1}$.

In our model studies, the Amazon forest area receives 3–4 Tg yr^{-1} . *Swap et al.* [1992] estimate that 14 Tg yr^{-1} of dust are deposited in the Amazon forest.

3.1.3. Yearly Variations

[44] Figure 3 shows global mass column burdens. There is a maximum in the Northern Hemisphere summer over Sahara and a maximum in the Northern Hemisphere spring in Asia. The Asian “spring dust” is a well-known phenomenon. The plume out of the western Sahara peaks in July, giving maximum transport across the Atlantic Ocean in the Northern Hemisphere summer. Loadings over Australia are low and peak in the Southern Hemisphere summer.

[45] A shift in the Atlantic plume is modeled. In Northern Hemisphere summer the plume is transported westward toward the Gulf of Mexico, whereas in Northern Hemisphere winter the plume is transported southwest toward the Amazon forest area [Prospero, 1996].

[46] Figure 4 shows zonal mean mass mixing ratios of dust. Dust is lifted higher in the Northern Hemisphere summer, when the deserts at 20°N are hottest. In July, significant amounts of dust are lifted above the 200 hPa level because of convection. In January, convection lifts dust only to about 600 hPa. The higher lifting is important for the interaction with terrestrial radiation. When dust is lifted high, it absorbs and re-emits longwave radiation at lower temperatures, giving a stronger longwave radiative effect than it would have at low levels.

3.1.4. Station Comparisons

[47] Model output from CTM2 has been compared to monthly mean mass concentrations from the University of Miami (RSMAS) network at several stations. The results are shown in Figure 5. For some stations we have concentrations from 1996 (Barbados, Bermuda, Miami, Izana, and Sal Island) and for the others, we only have climatological means (Jeju, Kaashidhoo, and Oahu). We compare grid cell

Table 3. Deposition to Oceans and Forests^a

Run	GOC	NATL	SATL	NPAC	SPAC	IND	MED	AMZ
MDSLNRPDF	382	103	78	18	8	106	53	4
MDSSQPDF	358	105	75	17	4	86	54	4
GEOPDF	359	95	85	23	9	84	42	4
TOPOPDF	457	94	68	23	6	198	53	3
MDSLNRMEAN	407	102	73	19	9	132	58	3

^aValues are given in Tg. The following abbreviations are used: GOC, global ocean; NATL, northern Atlantic Ocean; SATL, southern Atlantic Ocean; NPAC, northern Pacific; SPAC, southern Pacific; IND, Indian Ocean, Persian Gulf, and the Red Sea; MED, Mediterranean; and AMZ, Amazon forest.

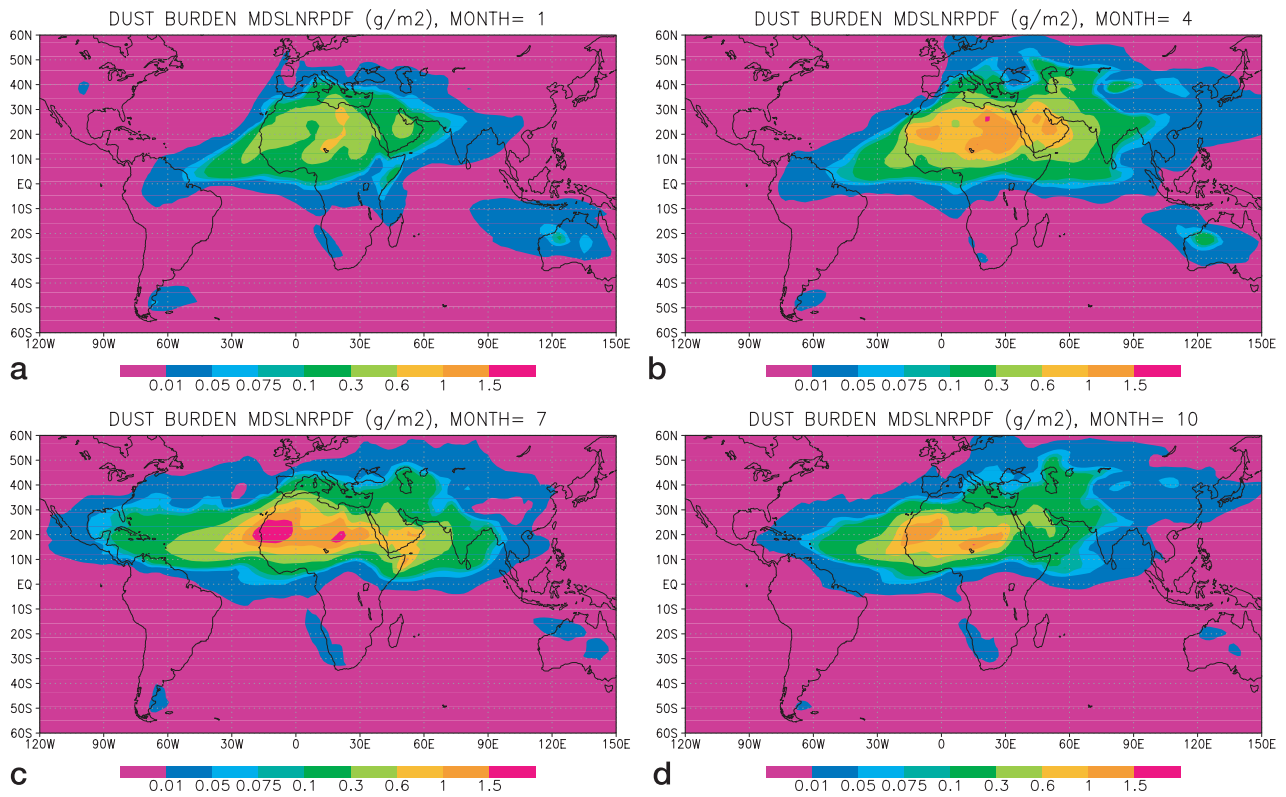


Figure 3. Seasonal variation in dust sources and transport as revealed by column burden in MDSLNRPDF experiment for (a) January, (b) April, (c) July, and (d) October.

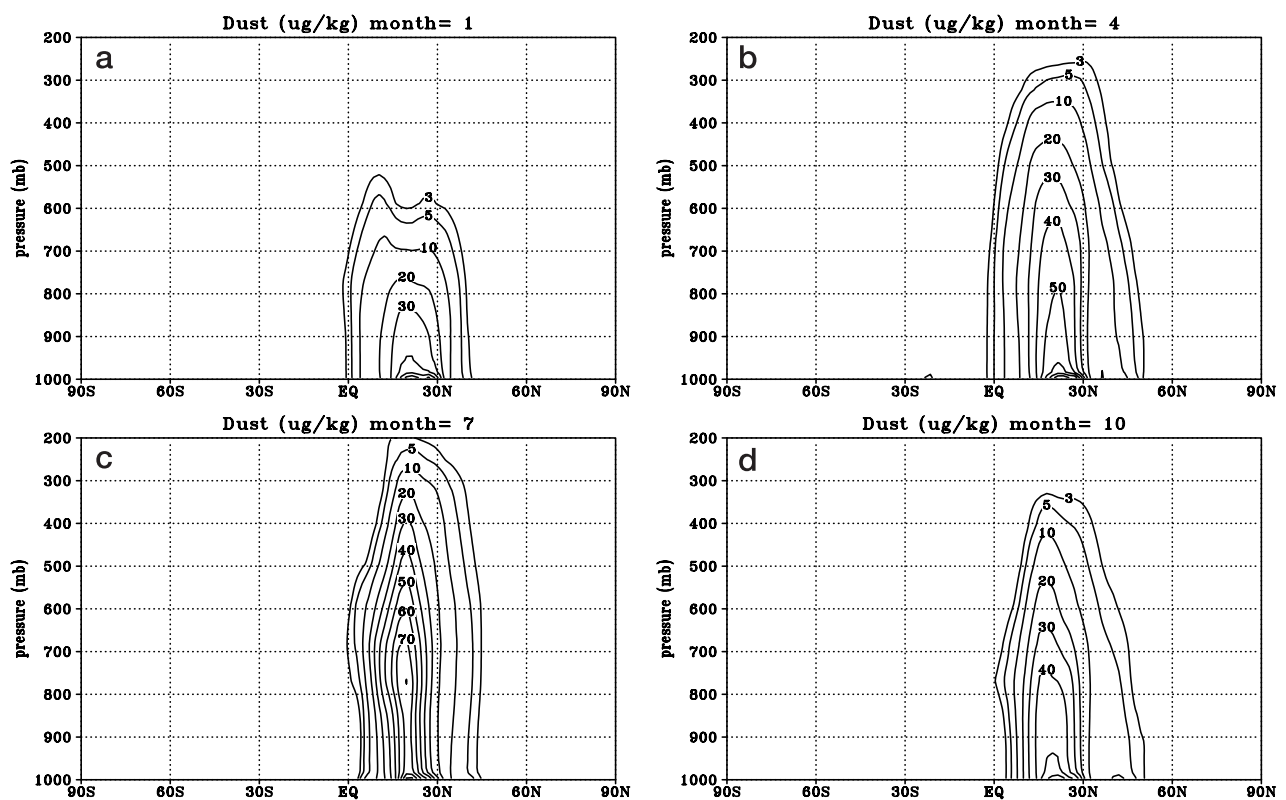


Figure 4. Zonal mean mass mixing ratio in MDSLNRPDF experiment for (a) January, (b) April, (c) July, and (d) October. Dust is transported much higher during Northern Hemisphere summer.

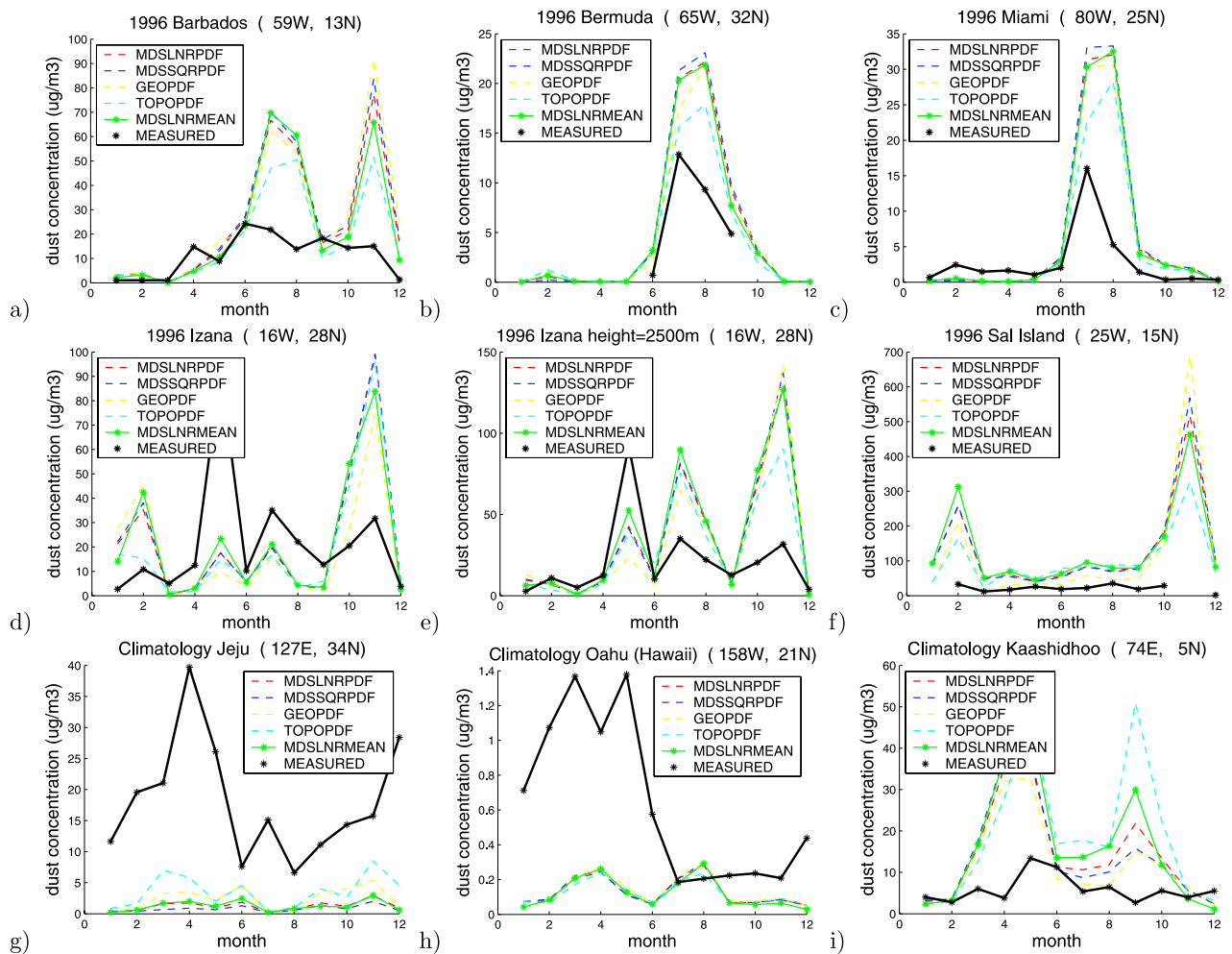


Figure 5. (a–i) Mass concentrations from University of Miami network compared to CTM2 concentrations. Note that Figures 5d and 5e are from the same station (Izana), but at different heights (see text). Black line is measurements. Red dashed line is MDSLNRPDF, blue dashed line is simulation MDSSQRPDF, yellow dashed line is simulation GEOPDF, cyan dashed line is simulation TOPOPDF, and green stars are simulation MDSLNRMEAN. When no black point is plotted, it means observations are missing.

mean simulations to in situ measurements, which may be influenced by local phenomena. However, it is necessary to verify that the model reproduces the seasonal cycle and the order of magnitude of the measured dust concentrations around the world.

[48] Figures 5a–5c show that Northern Hemisphere summer peaks at stations in the remote Atlantic plume are reasonably simulated. For the stations far from dust source regions (Barbados, Bermuda, and Miami), simulations show similar results with high summer dust concentrations. The model has a large outbreak in the Sahara in November, which is transported southwest to Barbados. This peak is not found in the measurements. The model reproduces phasing of the summertime peak in Miami and Bermuda and the wintertime minimum in Miami. This strong seasonal cycle results from stronger summer than winter emissions and from more northerly wintertime flow (see section 3.1.3). There are no measurements from Bermuda in January–May or in October–December.

[49] The model has difficulty predicting surface concentration at stations close to the African coast. Comparisons at Izana (Figures 5d–5e) improve when the model is sampled in the free troposphere (where the observatory is) rather than at sea level. The observatory at Sal Island is lower than Izana, but still above the lowest model layer. Section 3.4 shows that our optical depth simulation at Cape Verde is quite reasonable. Hence model biases in surface concentration do not imply biases in total column load. The vertical concentration gradient is difficult to predict close to source regions.

[50] The only Asian station to which we can compare the model output in 1996 is Jeju, where all our simulations underpredict dust (Figure 5g). Simulations GEOPDF and TOPOPDF best reproduce the observed concentrations. Situated south of Korea, Jeju should be dominated by Gobi dust since Tarim Basin dust is transported northwest [Sun *et al.*, 2001]. Either all Asian sources are too weak or the loss processes over China are too efficient.

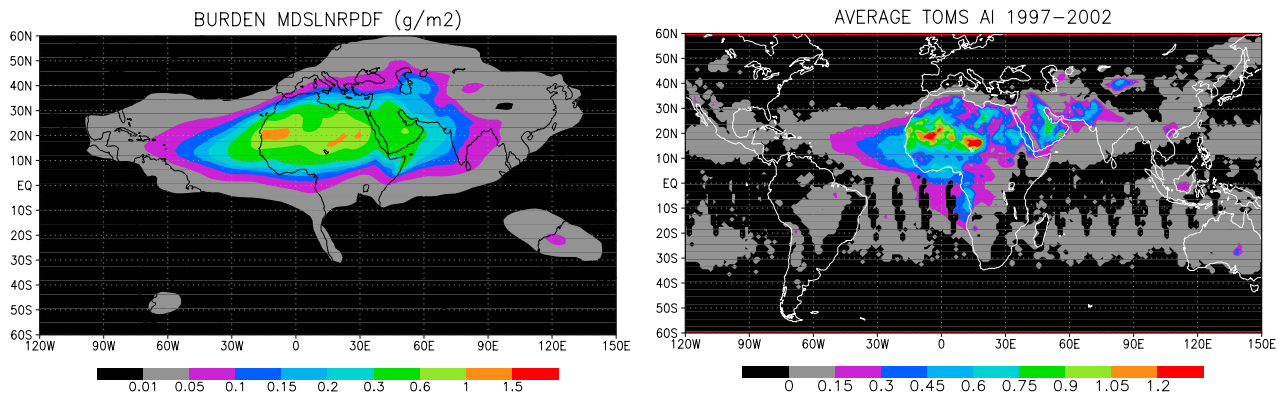


Figure 6. (left) Annual mean CTM2-simulated dust loading for 1996 and (right) mean TOMS aerosol index for 1997–2002.

[51] The model bias in Asian dust at Jeju is likely due to incorrect model sources or to representation of scavenging. In nature it may be that dust aerosols activate to cloud droplets less frequently over polluted Asia, where competition with other aerosols is stronger than over the more remote Atlantic. In our model, rain removes dust with a uniform efficiency ($\epsilon = 1$). Decreasing ϵ to 0.3 (equation (7)) increases concentrations at Jeju by approximately 100% (not shown). Testing this hypothesis would require a wet deposition scheme that represents competition among aerosols for in-cloud nucleation. This is beyond the scope of our model, though it is likely that ϵ in nature differs between the Atlantic dust plume and the Gobi region in Asia.

[52] The model concentrations are also too low at Oahu (Figure 5h). This is consistent with weak Asian sources or high loss during transport from China (see discussion above). Kaashidhoo (Figure 5i) is in the Maldives, south of India. Section 3.3.1 below shows that some simulations give too high concentrations and some give reasonable concentrations at Kaashidhoo.

3.2. Annual Average of MDSLNRPDF Run

[53] Figure 6 shows the similarity between the MDSLNRPDF simulation of 1996 and the mean TOMS aerosol index for 1997–2002 (TOMS data do not exist for 1996 until August). The MDSLNRPDF simulation reproduces many aspects of the TOMS observations, including the following: (1) two main Saharan dust regions, one over Mali in the western Sahara and one over the Bodele Depression–Lake Chad region in the southeastern Sahara; (2) the Takla Makan Desert, not the Gobi Desert, being the strongest Chinese dust source; (3) a source region near the Caspian Sea (compare Figure 2) and a source region in middle Saudi Arabia; and (4) low Australian sources as indicated by TOMS (Figure 6) (however, the model overestimates emissions from the Great Sandy Desert compared to TOMS).

3.3. Effect of Changed Dust Production

[54] We now discuss in detail the effect that using different assumptions has for a source region. Zender *et al.* [2003b] previously compared observations (including TOMS) with DEAD model simulations using several erodibility data sets. Figure 7 shows the differences between

simulation MDSLNRPDF and the others for dust production and burden.

3.3.1. Africa and the Atlantic Plume

[55] The monthly mean Atlantic plume seems relatively insensitive to the erodibility data set used (Figures 5a–5c). All model experiments reproduce summer peak monthly mean values at Miami, Bermuda, and Barbados. The TOPOPDF erodibility experiment yields the lowest concentrations at these stations, consistent with lowest loading over the Sahara in this run (Figure 7g).

[56] Figures 7b and 7c show that the GEOPDF and TOPOPDF erodibility simulations both produce higher emissions in the Bodele/Lake Chad region, consistent with TOMS. GEOPDF gives the highest burden of dust transported from this region. This dust is transported southwest, where it eventually mixes with biomass-burning aerosols [e.g., Chin *et al.*, 2002; Bian and Zender, 2003].

[57] The TOPOPDF and MDSLNRMEAN experiments produce high Somali emissions (Figures 7c and 7d), contrary to the TOMS aerosol index (Figure 6). This dust flows eastward in our model, producing high burdens over the Indian Ocean and high concentrations at Kaashidhoo (Figure 5). High soil erodibility produces strong Somali emissions in the TOPOPDF simulation. In the MDSLNRMEAN simulation, strong Somali emissions are due to redistribution of fixed annual emissions (1500 Tg) to coastal areas with strong winds. Areas that emit weakly with wind speed PDFs do not produce dust when only mean winds are used since the threshold wind is not reached. Fixing total emissions by changing the tuning factor in equation (1) puts these “lost” emissions in windy areas such as the Somali coast in the MDSLNRMEAN experiment.

[58] All experiments agree on high production in the western Sahara but disagree on the exact location. Figures 7a and 7d show that the reflectivity-based data sets give emissions mostly in mid-Mali/Mauritania whereas TOPOPDF and GEOPDF (Figures 7b and 7c) experiments produce more in northern Mali into Algeria. TOMS (Figure 6) indicates a maximum closer to the reflectivity-based experiments.

3.3.2. East Asia/China

[59] All model experiments underestimate the concentration at Jeju downwind of China (Figure 5g). These experi-

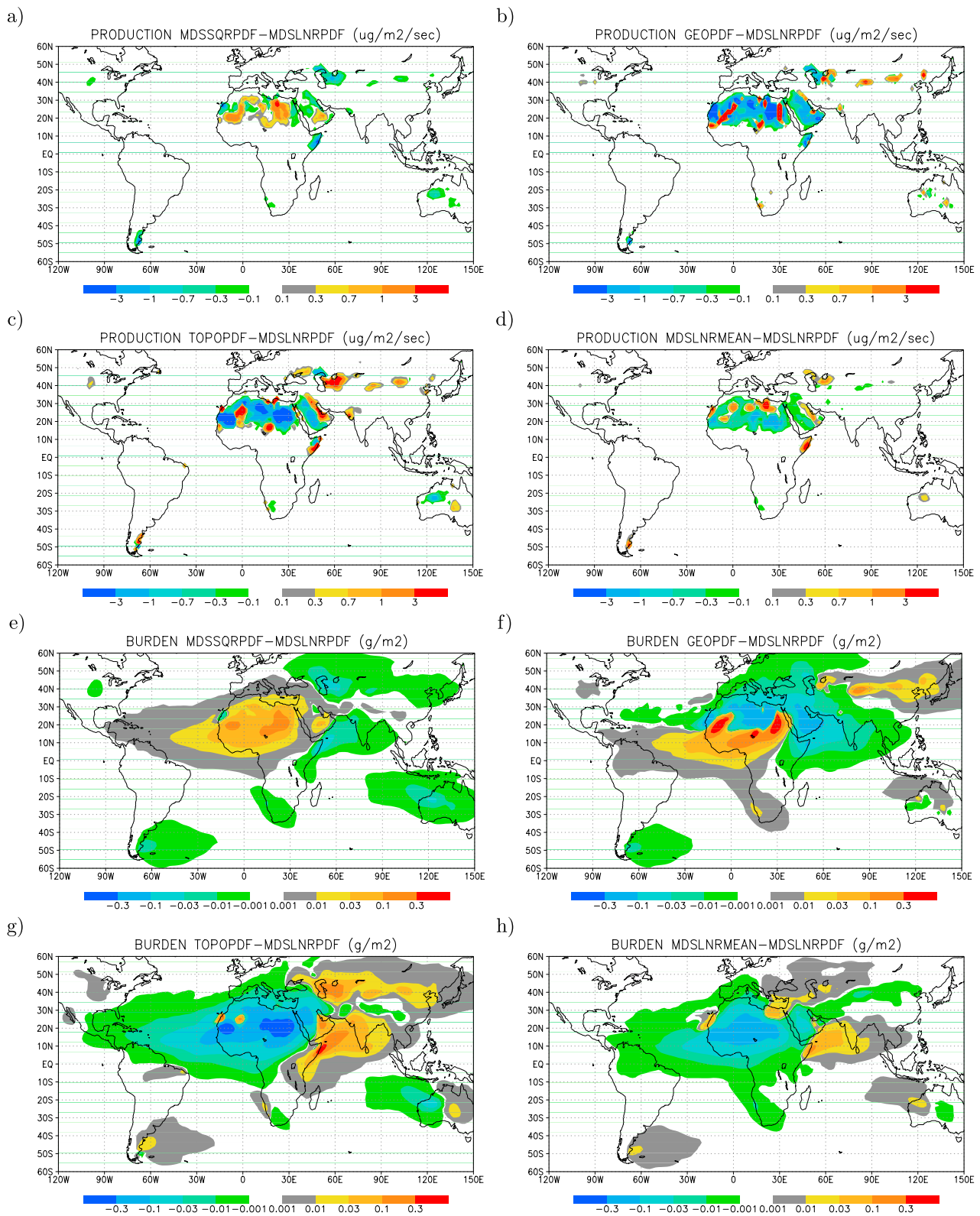


Figure 7. (a–h) Absolute difference in annual mean dust production and burden for all simulations. Differences are due to changing erodibility (MDSSQRPDF, TOPOPDF, and GEOPDF) or neglecting wind speed variability (MDSLNRMEAN).

ments have only two distinct areas for Chinese dust emissions, the Takla Makan and Gobi Deserts. However they disagree on the magnitude of the erodibility. The erodibility in Chinese source regions is low in the MDSLNR and MDSSQR erodibility factors since the reflectivity is divided by the global maximum reflectivity (SR_{\max} in equations (3) and (4)). The east Asian production is significantly higher in the TOPOPDF and GEOPDF experiments (Figures 7c and 7d). As mentioned above, low simulated concentrations at Jeju may be due to unrealistically strong deposition during transport from the Gobi region.

[60] TOMS indicates that the Takla Makan should be a more important source region than Gobi (Figure 6). *Shao et al.* [2003] argue that the Gobi was the more important source in spring 2002. Our study cannot conclusively answer this debate, yet it does make clear that contrary to North African emissions, east Asian emissions in these two deserts are very sensitive to the erodibility data set. *Zender et al.* [2003b] found that the GEO erodibility data set gave strong agreement with TOMS data for the Chinese deserts. All erodibility data sets in our study indicate high erodibility in the same regions (see Figure 1) yet disagree on the magnitude of the erodibility.

[61] Figure 7d shows that neglecting wind speed variability significantly lowers Chinese dust emissions. Possibly, it is a worse approximation to use large-scale mean winds in the smaller, more heterogeneous Chinese deserts than in the larger desert areas in the Sahara. The Takla Makan Desert is surrounded by 5000-m-high mountains [*Sun et al.*, 2001]. It is difficult for a large-scale CTM to capture the topographic effects on dust emissions in a landscape with such strong vertical gradients.

[62] The TOPOPDF and GEOPDF simulations (Figures 7b, 7c, 7f, and 7g) produce significantly higher emissions in China yet still fail to reproduce the observed concentrations at Jeju or Oahu. *Ginoux et al.* [2001] and *Luo et al.* [2003] both simulated reasonable concentrations at Jeju using TOPO erodibility and NASA/DAO and NCAR/NCEP meteorology combined with MATCH and GOCART transport models. It would be interesting to drive our CTM2 simulations with NASA/DAO or NCAR/NCEP meteorology to assess how the ECMWF meteorological data influence our results. However, such a comparison is beyond the scope of this study. As mentioned earlier (section 3.1.4), weaker scavenging efficiency (equation (7)) would give reasonable concentrations in east Asia or at Oahu (Hawaii) using GEOPDF or TOPOPDF source formulations.

3.3.3. Australia

[63] There are two potentially important dust sources in Australia, the Great Sandy Desert and the Lake Eyre basin (in Australia's northwest and southeast, respectively). All erodibility data sets show highest erodibility in the Lake Eyre basin (Figure 1), consistent with TOMS (Figure 6). Dust activity is known to occur in the Great Sandy Desert too [*Zender et al.*, 2003b].

[64] Nearly all Australian dust emerges from the Lake Eyre basin in the TOPOPDF experiment (Figure 7c). The other experiments produce dust from both sources. Neglecting wind speed variability (Figures 7d and 7h) produces much higher emissions in the Great Sandy Desert. As discussed earlier, neglecting wind speed variability increases dust in windy areas since emissions are replaced

from areas with high wind speeds to areas with low wind speeds when wind speed PDF is used. Our results suggest that high wind speeds drive emissions in the Great Sandy Desert, whereas high erodibility drives emissions in the Lake Eyre basin. Some earlier models [e.g., *Woodward*, 2001] show high emissions for the Great Sandy Desert, which may be due to favoring emissions from areas with high wind rather than high erodibility. Accounting for wind speed variability moves some emissions to areas with average winds lower than the threshold. Conclusively determining the relative magnitude of the two Australian sources would require observations other than TOMS.

3.3.4. Western Asia/Arabia

[65] All model experiments have emissions east of the Caspian Sea and south of the Aral Sea (Figures 2 and 7a–7d). TOMS indicates an only slightly elevated aerosol index east of the Caspian Sea (Figure 6). Figure 1 shows that the highest reflectivity occurs slightly south of the Aral Sea. We do not have any direct measurements to verify whether emissions are limited to the areas around the Caspian Sea, the Aral Sea, or both.

[66] The reflectivity-based erodibility factors produce strong emissions throughout the Saudi Arabian Ar Rub al Khali Desert. The GEO and TOPO erodibilities predict higher emissions in eastern Saudi Arabia, near the Persian Gulf and in southern Iraq (Figure 1), consistent with TOMS (Figure 6). Advection distributes the dust throughout this area, so determining the exact source regions from TOMS is difficult.

3.4. Optical Depths in the Western Saharan Plume

[67] To check if the choice of soil erodibility had a large effect on the simulation of specific dust episodes, we compare the daily observed and modeled optical depths at Cape Verde. Cape Verde (16°N , 22°W) lies amid the dust plume emanating from the western Sahara. The optical depth at Cape Verde is dominated by dust, although biomass-burning aerosols can be important here too [*Tanré et al.*, 2003]. Comparing optical depths rather than surface concentrations indicates whether the total column is correctly predicted and makes the comparison less sensitive to vertical concentration profiles.

[68] Table 4 shows correlation coefficients between each model experiment and the daily aerosol optical depth at Cape Verde. The erodibility factor strongly influences the results. The reflectivity-based erodibility experiments have high correlations (larger than 0.50). The small difference in correlation between MDSLNRPDF and MDSLNRMEAN indicates that the dust outbreak frequency close the source areas is insensitive to sub-grid-scale wind speed variability. This is consistent with *Grini and Zender* [2004], who simulated dust emissions during a period in the summer of 2000 and found that major outbreaks were well simulated independent of subgrid wind speed variability.

[69] Figure 8 (left) shows the aerosol optical depth at Cape Verde for the MDSLNRPDF, MDSSQRPDF, and MDSLNRMEAN simulations. Of the simulations representing wind speed PDFs, these reflectivity-based simulations have the highest correlation coefficients at Cape Verde. Both the magnitude and the timing of the observed events are well simulated.

Table 4. Aerosol Optical Depth at Cape Verde^a

	Mean	Standard Deviation	Correlation Coefficient
AERONET	0.37	0.25	
MDSLNRPDF	0.33 (0.33)	0.29 (0.27)	0.53
MDSSQRPDF	0.35 (0.35)	0.31 (0.29)	0.51
GEOPDF	0.36 (0.34)	0.43 (0.38)	0.38
TOPOPDF	0.25 (0.25)	0.24 (0.21)	0.47
MDSLNRMEAN	0.31 (0.30)	0.30 (0.28)	0.54

^aShown are mean value, standard deviation, and correlation coefficient for days when AERONET had measurements. Values for all days, including days without measurements, are given in parentheses.

[70] Figure 8 (right, note difference in scales) shows the GEOPDF and TOPOPDF results. When there are peaks in GEOPDF, the peaks are too large. GEOPDF predicts maxima much larger than observed. TOPOPDF generally underpredicts background optical depth. GEOPDF shows significantly lower correlation than the other simulations at Cape Verde. The geomorphologic erodibility devised by Zender *et al.* [2003b] does not perform well in this model on daily timescales in the western Sahara. The maxima in the GEOPDF simulation indicate that the GEO erodibility data set may be too heterogeneous.

[71] Among the experiments the western Sahara regions with highest erodibility are close neighbors. This makes attribution of major source areas difficult. The magnitude of dust outbreaks depends strongly on the erodibility, whereas the frequency of dust outbreaks is not influenced (see equation (1)). Exact representation of magnitude and frequency is less important when comparing to monthly mean concentrations since these effects average out and the emissions all come from approximately the same area (the western Sahara). When comparing to individual outbreaks, the choice of erodibility factor is more important. Studying individual outbreaks with the help of satellites, measurements from aircraft, and transport models can help to attribute the precise dust source regions.

4. Discussion

[72] Neglecting subgrid wind speed variability in dust production models generally results in lower emissions.

However, this and most other modeling studies tune global emissions to match global concentration or optical depth measurements. We fixed global emissions at 1500 Tg yr^{-1} in all experiments, so including wind speed PDFs redistributes emissions to areas that would not normally have enough wind to exceed the threshold for dust emission. This study clearly shows that neglecting wind PDFs gives higher emissions in areas where winds are high, such as coastal areas. Examples include Somalia, the Caspian Sea region, the Great Sandy Desert, the western coasts of Morocco and Mauritania, the Egyptian coast, and the eastern coast of South America (Figures 7d and 7h).

[73] Emissions strongly depend on the assumed erodibility factor. Several important conclusions can be drawn from our study: (1) The subtropical North Atlantic dust plume has approximately the same seasonal variation independent of erodibility factor. (2) Correct hindcasts of daily individual outbreaks into the subtropical North Atlantic are strongly sensitive to erodibility factors (Figure 8). (3) Reflectivity-based erodibility factors give better agreement with measurements for the important Cape Verde station in the Saharan dust plume. (4) Erodibility factors for the Chinese deserts are too low if calculated by scaling soil reflectivity to maximum soil reflectivity.

[74] The reflectivity-based erodibility factors that we propose are conceptually simple (equations (3) and (4)). They are consistent with the high reflectivity of sand dunes [Tsvetinskaya *et al.*, 2002], which are highly erodible. However, the erodibility cannot be expected to be directly connected to MDSLNR or MDSSQR in areas where sand

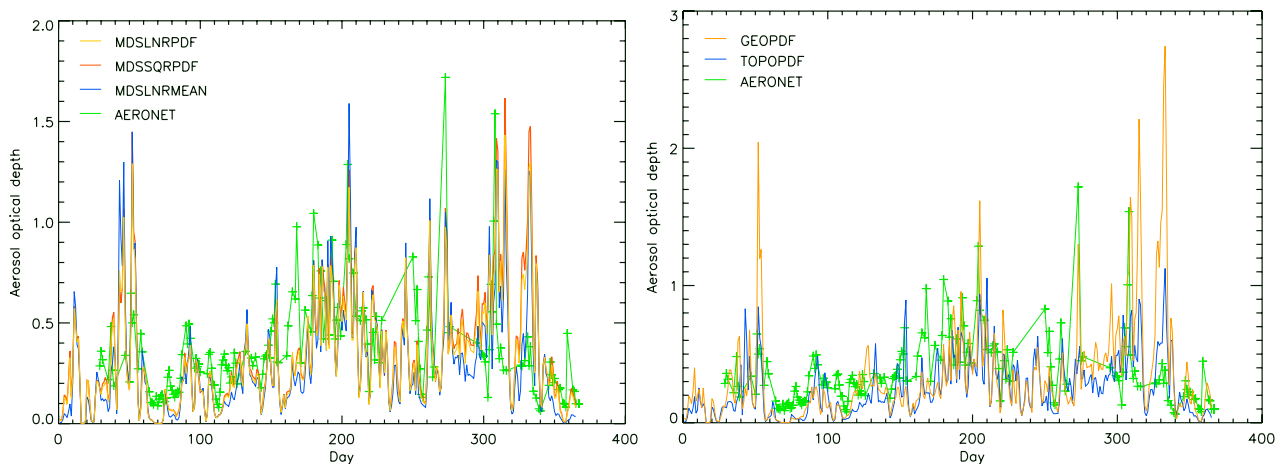


Figure 8. Aerosol optical depth at Cape Verde. The left figure compares MDSLNRPDF, MDSSQRPDF, and MDSLNRMEAN simulations to measurements. The right figure compares GEOPDF and TOPOPDF simulations to measurements. Note the difference in scale between left and right panels.

dunes are mixed with other soil types. For example, *Claquin et al.* [1999] calculated that dust originating from the Sahara would have higher single-scattering albedo than dust from other dust sources because of mineralogical differences. The reflectance-based erodibilities do not necessarily capture the enhanced erodibility of soil types other than dunes/shifting sand. Given their conceptual simplicity, the apparent success of these reflectance-based formulations in the western Sahara (Figure 8) is encouraging.

[75] The scarcity of observations in strategic dust hot spot regions makes it difficult to judge if our modeling results are realistic. In situ optical depth and concentration time series measurements from important regions such as the Bodele/Lake Chad, Somalia, Mali, Takla Makan, and the Caspian Sea are not available to us to evaluate our results. More campaigns observing individual outbreaks would be valuable for evaluating active source regions. Such campaigns should include measurements from aircraft, satellites, and modeling [e.g., *Myhre et al.*, 2003].

[76] Although the goal of our research is to better understand dust sources and production, we evaluate our experiments by comparing to measurements of dust concentrations and optical depth because no direct measurements of dust fluxes over large areas exist. Hence our conclusions are couched in uncertainty introduced by transport and loss processes.

[77] We use a simple formulation for wet deposition where the dust scavenging is proportional to the precipitated cloud liquid water fraction. This parameterization may not be suitable for dust, which may be insoluble. However, dust may become coated with water-soluble material and change properties during transport [*Fan et al.*, 2004]. Pristine dust types may also be slightly water-soluble depending on their carbonate content [*Claquin et al.*, 1999]. Interaction between aerosol and clouds is complicated and depends on the “background” aerosol concentration [*Ghan et al.*, 1998]. It is possible that dust can more easily interact with clouds over ocean than over land because of lower aerosol concentrations over ocean.

5. Summary

[78] Several different parameterizations of dust production and transport have been tested and evaluated. We focused on wind speed variability and soil erodibility. Both factors influence the magnitude and geographic location of dust emissions. Representing wind speed variability as a PDF changes the geographic pattern of dust emissions. In theory, representing wind speed variability increases production since emissions may occur at lower mean wind speeds. A consequence of fixing global production to a constant value is that areas with high wind speeds (for example, coastal areas) produce less dust when subgrid wind variability is represented.

[79] Dust source locations and strengths are strongly sensitive to soil erodibility. MODIS satellite data and the DEAD dust model show that soil reflectivity is a useful proxy for soil erodibility. In particular, the reflectivity-based erodibility performs well compared to other erodibility assumptions at predicting daily aerosol optical depth measurements in the Saharan plume. Reflectance-based erodibility hypotheses should be tested with other models and

meteorological analyses to determine whether these results are generic or model-specific.

[80] **Acknowledgments.** A.G., G.M., and I.S.A.I. acknowledge support from the Norwegian research council grant 139810/720 (CHEMCLIM) and from the Nordic Centre of Excellence, BACCI. C.S.Z. acknowledges support from NASA grants NAG5-10147 (IDS) and NAG5-10546 (NIP). Two anonymous reviewers helped improve this manuscript.

References

- Berglen, T. F., T. K. Berntsen, I. S. A. Isaksen, and J. K. Sundet (2004), A global model of the coupled sulfur/oxidant chemistry in the troposphere: The sulfur cycle, *J. Geophys. Res.*, *109*, D19310, doi:10.1029/2003JD003948.
- Bian, H., and C. S. Zender (2003), Mineral dust and global tropospheric chemistry: Relative roles of photolysis and heterogeneous uptake, *J. Geophys. Res.*, *108*(D21), 4672, doi:10.1029/2002JD003143.
- Cakmur, R. V., R. L. Miller, and O. Torres (2004), Incorporating the effect of small-scale circulations upon dust emissions in an atmospheric general circulation model, *J. Geophys. Res.*, *109*, D07201, doi:10.1029/2003JD004067.
- Chin, M., et al. (2002), Tropospheric aerosol optical thickness from the GOCART model and comparisons with satellite and Sun photometer measurements, *J. Atmos. Sci.*, *59*, 461–483.
- Claquin, T. (1999), Modelisation de la mineralogie et du forçage radiatif des poussières desertiques, Ph.D. thesis, Univ. of Hamburg, Hamburg, Germany.
- Claquin, T., M. Schulz, and Y. Balkanski (1999), Modeling the mineralogy of atmospheric dust sources, *J. Geophys. Res.*, *104*(D18), 22,243–22,256.
- D’Almeida, G. A. (1987), On the variability of desert aerosol radiative characteristics, *J. Geophys. Res.*, *92*(D3), 3017–3026.
- Endresen, Ø., E. Søgård, J. K. Sundet, S. B. Dalsøren, I. S. A. Isaksen, T. F. Berglen, and G. Gravr (2003), Emission from international sea transportation and environmental impact, *J. Geophys. Res.*, *108*(D17), 4560, doi:10.1029/2002JD002898.
- Fan, S., L. W. Horowitz, H. Levy II, and W. J. Moxim (2004), Impact of air pollution on wet deposition of mineral dust aerosols, *Geophys. Res. Lett.*, *31*, L02104, doi:10.1029/2003GL018501.
- Fecan, F., B. Marticorena, and G. Bergametti (1999), Parameterization due to the increase of the aeolian erosion threshold wind friction velocity due to soil moisture for arid and semi-arid areas, *Ann. Geophys.*, *17*, 149–157.
- Gauss, M., I. S. A. Isaksen, S. Wong, and W.-C. Wang (2003), Impact of H₂O emissions from cryoplanes and kerosene aircraft on the atmosphere, *J. Geophys. Res.*, *108*(D10), 4304, doi:10.1029/2002JD002623.
- Ghan, S., G. Guzman, and H. Abdul-Razzak (1998), Competition between sea salt and sulfate particles as cloud condensation nuclei, *J. Atmos. Sci.*, *55*, 3340–3347.
- Gillette, D. (1999), A qualitative geophysical explanation for “hot spot” dust emitting source regions, *Beitr. Phys. Atmos.*, *72*, 67–77.
- Ginoux, P., M. Chin, I. Tegen, J. M. Prospero, B. Holben, O. Dubovik, and S.-J. Lin (2001), Sources and distributions of dust aerosols simulated with the GOCART model, *J. Geophys. Res.*, *106*(D17), 20,255–20,273.
- Grini, A., and C. S. Zender (2004), Roles of saltation, sandblasting, and wind speed variability on mineral dust aerosol size distribution during the Puerto Rican Dust Experiment (PRIDE), *J. Geophys. Res.*, *109*, D07202, doi:10.1029/2003JD004233.
- Grini, A., G. Myhre, J. Sundet, and I. S. A. Isaksen (2002), Modeling the annual cycle of sea salt in the global 3D model Oslo CTM2: Concentrations, fluxes and radiative impact, *J. Clim.*, *15*, 1717–1730.
- Iversen, J., and B. White (1982), Saltation threshold on Earth, Mars and Venus, *Sedimentology*, *29*, 111–119.
- Justus, C., W. Hargraves, A. Mikhail, and D. Graber (1978), Methods for estimating wind speed frequency distributions, *J. Appl. Meteorol.*, *17*, 350–353.
- Lohmann, U. (2002), Possible aerosol effects on ice clouds via contact nucleation, *J. Atmos. Sci.*, *59*, 647–656.
- Luo, C., N. M. Mahowald, and J. del Corral (2003), Sensitivity study of meteorological parameters on mineral aerosol mobilization, transport, and distribution, *J. Geophys. Res.*, *108*(D15), 4447, doi:10.1029/2003JD003483.
- Mahowald, N. M., R. G. Bryant, J. del Corral, and L. Steinberger (2003), Ephemeral lakes and desert dust sources, *Geophys. Res. Lett.*, *30*(2), 1074, doi:10.1029/2002GL016041.
- Marticorena, B., and G. Bergametti (1995), Modeling of the atmospheric dust cycle: I. Design of a soil-derived dust emission scheme, *J. Geophys. Res.*, *100*(D8), 16,415–16,430.

- Myhre, G., and F. Stordal (2001), Global sensitivity experiments of the radiative forcing due to mineral aerosols, *J. Geophys. Res.*, *106*(D16), 18,193–18,204.
- Myhre, G., A. Grini, J. M. Haywood, F. Stordal, B. Chatenet, D. Tanré, J. K. Sundet, and I. S. A. Isaksen (2003), Modeling the radiative impact of mineral dust during the Saharan Dust Experiment (SHADE) campaign, *J. Geophys. Res.*, *108*(D18), 8579, doi:10.1029/2002JD002566.
- Nenes, A., S. Ghan, H. Abdul-Razzak, P. Chuang, and J. Seinfeld (2001), Kinetic limitations on cloud droplet formation and impact on cloud albedo, *Tellus, Ser. B*, *53*, 133–149.
- Prather, M. J. (1986), Numerical advection by conservation of second-order moments, *J. Geophys. Res.*, *91*(D6), 6671–6681.
- Prospero, J. (1996), The atmospheric transport of particles to the ocean, in *Particle Flux in the Ocean*, edited by V. Ittekkot et al., pp. 19–53, John Wiley, Hoboken, N. J.
- Prospero, J. M., P. Ginoux, O. Torres, S. E. Nicholson, and T. E. Gill (2002), Environmental characterization of global sources of atmospheric soil dust identified with the Nimbus 7 Total Ozone Mapping Spectrometer (TOMS) absorbing aerosol product, *Rev. Geophys.*, *40*(1), 1002, doi:10.1029/2000RG000095.
- Schaaf, C., et al. (2002), First operational BRDF, albedo nadir reflectance products from MODIS, *Remote Sens. Environ.*, *83*, 135–148.
- Seinfeld, J. H., and S. N. Pandis (1998), *Atmospheric Chemistry and Physics: From Air Pollution to Climate Change*, John Wiley, Hoboken, N. J.
- Shao, Y., et al. (2003), Northeast Asian dust storms: Real-time numerical prediction and validation, *J. Geophys. Res.*, *108*(D22), 4691, doi:10.1029/2003JD003667.
- Sherwood, S. (2002), A microphysical connection among biomass burning, cumulus clouds and stratospheric moisture, *Science*, *295*, 1272–1275.
- Sun, J., M. Zhang, and T. Liu (2001), Spatial and temporal characteristics of dust storms in China and its surrounding regions, 1960–1999: Relations to source area and climate, *J. Geophys. Res.*, *106*(D10), 10,325–10,333.
- Sundet, J. K. (1997), Model studies with a 3-D global CTM using ECMWF data, Ph.D. thesis, Univ. of Oslo, Oslo.
- Swap, R., M. Garstang, and S. Greco (1992), Saharan dust in the Amazon Basin, *Tellus, Ser. B*, *44*, 133–149.
- Tanré, D., J. Haywood, J. Pelon, J. F. Lon, B. Chatenet, P. Formenti, P. Francis, P. Goloub, E. J. Highwood, and G. Myhre (2003), Measurement and modeling of the Saharan dust radiative impact: Overview of the Saharan Dust Experiment (SHADE), *J. Geophys. Res.*, *108*(D18), 8574, doi:10.1029/2002JD003273.
- Tegen, I., and I. Fung (1994), Modeling of mineral dust in the atmosphere: Sources, transport and optical thickness, *J. Geophys. Res.*, *99*(D11), 22,897–22,914.
- Tegen, I., S. P. Harrison, K. Kohfeld, I. C. Prentice, M. Coe, and M. Heimann (2002), Impact of vegetation and preferential source areas on global dust aerosol: Results from a model study, *J. Geophys. Res.*, *107*(D21), 4576, doi:10.1029/2001JD000963.
- Tiedtke, M. (1989), A comprehensive mass flux scheme for cumulus parameterization on large scale models, *Mon. Weather Rev.*, *117*, 1779–1800.
- Tsvetinskaya, E. A., C. B. Schaaf, F. Gao, A. H. Strahler, R. E. Dickinson, X. Zeng, and W. Lucht (2002), Relating MODIS-derived surface albedo to soils and rock types over northern Africa and the Arabian Peninsula, *Geophys. Res. Lett.*, *29*(9), 1353, doi:10.1029/2001GL014096.
- Viterbo, P., and A. C. Beljaars (1995), An improved land surface parameterization scheme in the ECMWF model and its validation, *J. Clim.*, *8*, 2716–2748.
- Woodward, S. (2001), Modeling the atmospheric life cycle and radiative impact of mineral dust in the Hadley Center climate model, *J. Geophys. Res.*, *106*(D16), 18,155–18,166.
- Zender, C. S., H. Bian, and D. Newman (2003a), Mineral Dust Entrainment and Deposition (DEAD) model: Description and 1990s dust climatology, *J. Geophys. Res.*, *108*(D14), 4416, doi:10.1029/2002JD002775.
- Zender, C. S., D. Newman, and O. Torres (2003b), Spatial heterogeneity in aeolian erodibility: Uniform, topographic, geomorphic, and hydrologic hypotheses, *J. Geophys. Res.*, *108*(D17), 4543, doi:10.1029/2002JD003039.

A. Grini, I. S. A. Isaksen, and G. Myhre, Department of Geosciences, University of Oslo, P. O. Box 1022, Blindern, N-0315 Oslo, Norway. (alf.grini@geo.uio.no; i.s.a.isaksen@geo.uio.no; gunnar.myhre@geo.uio)

C. S. Zender, Department of Earth System Science, University of California, Irvine, 205 Physical Sciences Research Facility, Irvine, CA 92697-3100, USA. (zender@uci.edu)